Mon. Not. R. Astron. Soc. **000**, 1–8 (2006) Printed 15 April 2008 (MN LaTeX style file v2.2)

arXiv:0804.2344v1 [astro-ph] 15 Apr 2008

Covariance of dark energy parameters and sound speed constraints from large HI surveys

A. Torres-Rodríguez[1], C. M. Cress[2], K. Moodley[1]
[1] *Astrophysics and Cosmology Research Unit, University of KwaZulu-Natal, Westville, 4000, South Africa*
[2] *Physics Department, University of the Western Cape, Cape Town 7535, South Africa*

15 April 2008

ABSTRACT
An interesting probe of the nature of dark energy is the measure of its sound speed, c_s. We review the significance for constraining sound speed models of dark energy using large neutral hydrogen (HI) surveys with the Square Kilometre Array (SKA). Our analysis considers the effect on the sound speed measurement that arises from the covariance of c_s with the dark energy density, $\Omega_{\rm de}$, and a time-varying equation of state, $w(a) = w_0 + (1-a)w_a$. We find that the approximate degeneracy between dark energy parameters that arises in power spectrum observations is lifted through redshift tomography of the HI-galaxy angular power spectrum, resulting in sound speed constraints that are not severely degraded. The cross-correlation of the galaxy and the integrated Sachs-Wolfe (ISW) effect spectra contributes approximately 10 percent of the information that is needed to distinguish variations in the dark energy parameters, and most of the discriminating signal comes from the galaxy auto-correlation spectrum. We also find that the sound speed constraints are weakly sensitive to the HI bias model. These constraints do not improve substantially for a significantly deeper HI survey since most of the clustering sensitivity to sound speed variations arises from $z \lesssim 1.5$. A detection of models with sound speeds close to zero, $c_s \lesssim 0.01$, is possible for dark energy models with $w \gtrsim -0.9$.

Key words: cosmological parameters - large-scale structure of the universe - cosmic microwave background - radio lines: galaxies

1 INTRODUCTION

The observed acceleration of the cosmic expansion has challenged our understanding of the composition and evolution of the universe. Evidence supporting the idea that about two-thirds of the energy in the universe is in the form of dark energy driving this acceleration has arisen from observations of type Ia supernovae (Riess et al. 1998; Perlmutter et al. 1999) and from a combination of large-scale structure (Tegmark et al. 2006) and cosmic microwave background (CMB) observations (Spergel et al. 2007).

Theoretical explanations of the observed acceleration can broadly be classified into three categories (Bean, Carrol & Trodden 2005). Firstly, there are models that remove the need for a new exotic component by seeking alternatives to dark energy, for example, by modifying gravity on cosmological scales (e.g. Dvali, Gabadadze & Porrati 2000; Deffayet 2001; Deffayet, Dvali & Gabadadze 2002; Carroll et al. 2005; Capozziello et al. 2006, also see Bean et al. (2007) and references therein). Alternatively, if one assumes the validity of general relativity and interprets the observational evidence as that for dark energy, the simplest theoretical explanation is that of the cosmological constant (Λ), whose main difficulty is the dramatic inconsistency between its measured value and the predicted value from quantum field theory (Weinberg 1989; Carroll 2001). The third category includes dynamical dark energy theories such as quintessence (e.g. Peebles & Ratra 1988; Ratra & Peebles 1988; Wetterich 1988; Ferreira & Joyce 1997; Caldwell, Dave & Steinhardt 1998, also see Linder (2007) and references therein) and k-essence models (Armendariz-Picon, Mukhanov & Steinhardt 2000, 2001; Chiba, Okabe & Yamaguchi 2000; Chiba 2002).

In dynamical dark energy theories, dark energy is typically modelled as a scalar field, with k-essence differing from quintessence in that it has a non-canonical kinetic term in the Lagrangian. The mechanism by which quintessence comes to dominate at later times, generating the accelerated expansion, is not clearly identified, leading to the so-called coincidence problem. The k-essence models were proposed to explain the late-time domination in a more natural way. Recently it has been claimed that k-essence models are not physical because in order to solve the coincidence problem in these models the speed of sound of dark energy, $c_s^2 = \delta p/\delta\rho$, has to be greater than unity in some epoch (Bonvin, Caprini & Durrer 2006, 2007) which violates causality. Other authors, however, (e.g. Kang, Vanchurin & Winitzki 2007; Babichev, Mukhanov & Vikman 2007) have argued that superluminal sound speed propagation does not lead to causality violation. There also exist k-essence models in which the sound speed is always less than unity but these do not appear to solve the coincidence problem (Scherrer 2004, 2006).

While the viability of k-essence models is debated, it is nevertheless useful to consider experiments which could distinguish between this type of dark energy model and quintessence. The sound speed for quintessence is always unity so that, as in the case of the cosmological constant, the quintessence field is expected to have no significant density fluctuations within the causal horizon, consequently it should contribute little to the clustering of matter in large-scale structure (Ferreira & Joyce 1998). In k-essence models, however, the sound speed is not unity and dark energy can cluster, thereby affecting the growth of large-scale structure. The detection of a signature of sound speed in the integrated Sachs Wolfe (ISW) effect as well as in the clustering of matter, can therefore provide valuable insight into the nature of dark energy.

Many experiments have been proposed to probe the properties of dark energy. While many have pursued constraining its equation of state, $w = p/\rho$, for example, using cluster counts surveys (Haiman, Mohr & Holder 2001; Weller, Battye & Kneissl 2002), baryon acoustic oscillations (Blake & Glazebrook 2003; Hu & Haiman 2003; Cooray 2004), weak lensing (Huterer 2002; Takada & Jain 2004; Song & Knox 2004) and type Ia supernova experiments (e.g. Weller & Albrecht 2002; Nesseris & Perivolaropoulos 2005), only a few have considered the prospects for sound speed detection (Hu & Scranton 2004; Dedeo, Caldwell & Steinhardt 2004; Weller & Lewis 2003; Hannestad 2005; Bean & Doré 2004; Corasaniti, Giannantonio & Melchiorri 2005). In Torres-Rodríguez & Cress (2007, hereafter TRC07), we studied the potential for combining data from the Square Kilometer Array (SKA[1]) with forthcoming Planck[2] data to measure the sound speed. Assuming the SKA will provide a redshift survey of 21-cm emitting galaxies over most of the sky out to z ~ 2, and a specific model for the evolution of HI in galaxies, we considered a combination of the galaxy auto-correlation and the galaxy-CMB cross-correlation in several cosmic epochs to trace the evolution of clustering. This evolution is somewhat sensitive to the sound speed of dark energy in the low-sound-speed regime. The cross-correlation signals are dominated by contributions from the ISW effect and thus provide a probe of the evolution of potentials on large scales where clustering of dark energy could be most noticeable. We found that for models with constant w, given high precision measurements of other cosmological parameters, it was possible to measure the effects of a sound speed that is much smaller than unity.

In this paper we extend our analysis to study the covariance of the sound speed with other dark energy parameters, particularly w_0, w_a and $\Omega_{\rm de}$. Since there are degeneracies in the parameter space when using the ISW effect and the clustering of HI galaxies as observables, it is important to consider the effect that uncertainties in these parameters have on the sound speed forecasts. For example, increasing the density of dark energy produces a larger suppression of the gravitational potential but this can be compensated by making the nature of dark energy more like matter by reducing its sound speed. Similarly, a lower value of w boosts the ISW effect at recent times but this can be compensated by reducing the sound speed of dark energy. We implement a Fisher matrix analysis to study the covariance between the dark energy parameters and calculate the significance for ruling out dark energy models with constant sound speed much less than that of canonical models. In particular, many k-essence models have low sound speeds for most of the period between last scattering and the present epoch (Erickson et al. 2002).

We also study the sensitivity of the sound speed constraints to different models for the HI bias, which has a direct impact on the galaxy power spectrum. Recently there has been discussion of radio telescopes other than the SKA which could carry out deep HI-galaxy redshift surveys over the same area of sky, and which could potentially be built before the multi-purpose SKA. We investigate how constraints on the sound speed improve for a much deeper HI-galaxy redshift survey.

The outline of the paper is as follows. In §2 we present the ISW and galaxy observables. In §3 we revise the properties of our model HI redshift distribution and the HI bias. In §4 we describe the statistical method used to derive parameter constraints and its numerical implementation. Finally, the results are presented and discussed in §5 with conclusions drawn in §6.

2 THEORY

2.1 Observables

We first review the ISW and HI-galaxy clustering observables which are used to discriminate dark energy models. More details can be found in TRC07.

The fluctuations in the matter distribution of the large-scale structure can be expressed in terms of the projected fractional source count of the mass tracer

$$\begin{aligned}\frac{\delta N}{N_0}(\hat{n}) &= \int_0^z b_{HI}(z)\,\frac{d\tilde{N}}{dz}\,\delta_m(z,\hat{n})\,dz \\ &= \delta_m^0(\hat{n})\int_0^z b_{HI}(z)\,\frac{d\tilde{N}}{dz}D(z)\,dz\,, \qquad (1)\end{aligned}$$

where b_{HI} is the linear bias parameter of the HI-galaxy population, δ_m is the matter overdensity ($\delta_m^0 \equiv \delta_m(z=0)$), $d\tilde{N}/dz$ is the normalised redshift distribution of HI galaxies and $D(z)$ is the linear growth of matter fluctuations given by $D(z) = \delta_m(z)/\,\delta_m^0$.

The Fourier modes of the temperature fluctuations originating from the ISW effect are expressed as the change in the gravitational potential over conformal time (or comoving distance, r) integrated from today to the epoch of decoupling

---

[1] `http://www.skatelescope.org/`

[2] `http://www.rssd.esa.int/index.php?project=PLANCK`

$$\begin{aligned}\frac{\delta T}{T_0}(k) &= -2\int_0^{r_{dec}} dr\,\Phi'(r,k)\\ &= \frac{3H_0^2\Omega_m}{c^2k^2}\,\delta_m^0(k)\int_0^z\frac{dg(z)}{dz}\,dz\,, \qquad (2)\end{aligned}$$

where H_0 and Ω_m are, respectively, the value of the Hubble constant and the matter density parameter today, Φ is the Newtonian gravitational potential, $\delta_m^0(k)$ is the Fourier transform of the matter distribution and the prime denotes derivatives with respect to comoving distance. The dominant contribution to the ISW effect comes from the CDM perturbations. This allows us to express the evolution of the gravitational potential as the change of the linear growth suppression factor, $g(z)=(1+z)D(z)$, via the Poisson equation.

We can express the galaxy auto-correlation, CMB auto-correlation and galaxy-CMB cross-correlation in harmonic space via their respective angular power spectra as

$$\begin{aligned}C_\ell^{gg} &= 4\pi\int\frac{dk}{k}\left\langle\Big|\frac{\delta N}{N_0}(k)\Big|^2\right\rangle j_\ell^2(kr)\\ &= 4\pi\int_0^\infty\frac{dk}{k}\,[f_\ell^N(k)]^2\Delta_m^2(k)\,, \qquad (3)\\ C_\ell^{TT} &= 4\pi\int\frac{dk}{k}\left\langle\Big|\frac{\delta T}{T_0}(k)\Big|^2\right\rangle j_\ell^2(kr)\\ &= 4\pi\int_0^\infty\frac{dk}{k}\,[f_\ell^T(k)]^2\Delta_m^2(k)\,, \qquad (4)\\ C_\ell^{gT} &= 4\pi\int\frac{dk}{k}\left\langle\frac{\delta N}{N_0}(k)\frac{\delta T}{T_0}(k)\right\rangle j_\ell^2(kr)\\ &= 4\pi\int_0^\infty\frac{dk}{k}\,f_\ell^N(k)f_\ell^T(k)\Delta_m^2(k)\,, \qquad (5)\end{aligned}$$

where $j_\ell(kr)$ is the spherical Bessel function and $\Delta_m^2(k)=k^3P_\delta(k)/2\pi^2$ is the logarithmic matter power spectrum today with $P_\delta(k)=\langle|\delta_m^0(k)|^2\rangle$. The functions $f_\ell^N(k)$ and $f_\ell^T(k)$ correspond to the weight functions for the HI survey and the ISW spectra respectively. They depend on both the redshift distribution of the galaxy selection function and the rate of change of the gravitational potential according to the cosmological model of dark energy. From Eqs. (1, 2) the weight functions are defined as

$$\begin{aligned}f_\ell^N(k) &= \int_0^z b_{HI}(z)\frac{d\tilde N}{dz}D(z)\,j_\ell(kr(z))\,dz\,, \qquad (6)\\ f_\ell^T(k) &= \frac{3H_0^2\Omega_m}{c^2k^2}\int_0^z\frac{dg(z)}{dz}\,j_\ell(kr(z))\,dz. \qquad (7)\end{aligned}$$

2.2 The effect of dark energy on the observables

The background expansion of the Universe is affected by the density of the matter component and by the equation of state parameter, w, through the Hubble parameter, $H(z)$. This modifies the comoving distance, r, and has a direct effect on Eqs. (3–5).

In a general fluid description for the density perturbations of dark energy (e.g. Bean & Doré 2004), the evolution of the fluctuations is characterised by both the equation of state and the speed of sound. In the frame where cold dark matter (CDM) is at rest, the evolution of the density and velocity perturbation of a general matter component (denoted by subscript i) is given by (Weller & Lewis 2003)

$$\begin{aligned}&\delta_i'+3\mathcal{H}(\hat c_{s,i}^2-w_i)(\delta_i+3\mathcal{H}(1+w_i)v_i/k)+\\ &\quad(1+w_i)kv_i+3\mathcal{H}w'v/k=-3(1+w_i)h' \qquad (8)\\ &\quad v_i'+\mathcal{H}(1-3\hat c_{s,i}^2)v_i=k\hat c_{s,i}^2\delta_i/(1+w_i)\,, \qquad (9)\end{aligned}$$

where $\mathcal{H}$ is the conformal Hubble parameter, v_i is the velocity, h' the synchronous metric perturbation (Ma & Bertschinger 1995) and the circumflex (ˆ) means the sound speed is defined in the rest frame of the dark energy component. Eq. (8) includes the variations of w with respect to conformal time. We consider models of dark energy with a slowly varying equation of state parameterized (Linder 2003) as a function of the scale factor, a:

$$w(a)=w_0+(1-a)w_a. \qquad (10)$$

We note that $\Omega_{\rm de}$ only appears directly in the background expansion, unlike $w(a)$ which, together with c_s, has a direct contribution to the density evolution. As we will see later, this has an effect on the covariance of these parameters.

3 THE HI-GALAXY SURVEY

In TRC07 we presented the motivation for using an experiment like the SKA to complete a large HI survey. There are some constraints on the distribution of HI gas at high redshift from Ly-α absorption studies (Péroux et al. 2003) but there remains a great deal of uncertainty in the HI selection function at high redshift. As our reference model, we adopt the model 'C' in Abdalla & Rawlings (2005) and investigate the impact of changing the selection function by, firstly, changing the integration time and, secondly, changing our assumption about the evolution of the HI bias.

For a single-pointing survey, a field of view (FOV) frequency dependence of ν^{-2} and a detection threshold of $S/N=10$, the number of HI galaxies per square degree, per redshift interval and at redshift z is expected to be reasonably approximated by

$$\frac{dN}{dz}=\mathcal{A}\,z\exp\left(\frac{-(z-z_c)^2}{2\,\sigma_z^2}\right), \qquad (11)$$

where the fitting parameters $\mathcal{A}$, z_c and σ_z depend on the integration time. We would like to investigate the performance of two different surveys: one of 4 hours of integration time per pointing (as in TRC07) and an ultra deep survey, using 36 hours of integration. We assume that both surveys are completed by an SKA-like experiment and cover the same area of sky but that the latter survey takes nine times longer to complete. Both survey selection functions are depicted in Fig. 1.

The selection function of our mass tracer is then $\phi(z)=b_{\rm HI}(z)\times{\rm d}\tilde N/dz$, where the tilde represents the normalised distribution over the redshift of interest. In order to increase the significance of distinguishing models, we divide the galaxy selection function into several redshift bins of width $\Delta z=0.2$ up to $z_{\max}=2$ (or $z_{\max}=3$ for the deeper survey), the width of redshift bin being chosen to minimise shot noise from a small number of galaxies in narrow bins and smearing of the gravitational potential along the line of sight in wide bins. We consider the galaxy and

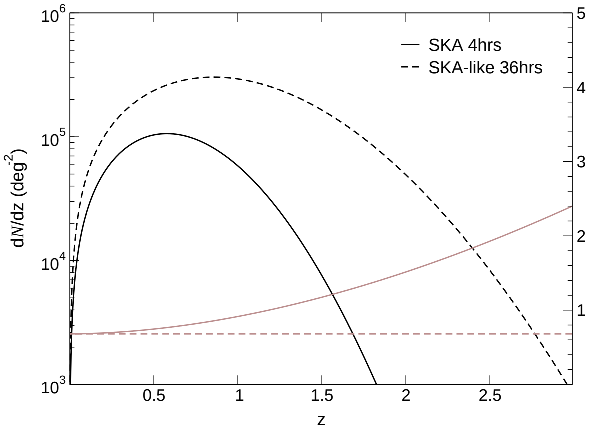

Figure 1. SKA redshift distributions of HI galaxies and models for the HI bias parameter used. An integration time for a single pointing of 36 hours (black dashed line) would reach a depth of $z = 3$. Taken from Basilakos et al. (2007), the two models for the HI bias (in grey) only differ greatly at high redshift. A constant bias model (grey dashed line) is unlikely to be realistic.

the ISW-galaxy power spectra in each bin as independent measurements.

From Eq. (6), we see that the bias factor has a direct impact on the galaxy-galaxy spectra. The effect of the bias model on the sound speed constraints is not straightforward to see, so we investigated this further by using different bias models. We have used two models for b_{HI} based on the studies of Basilakos et al. (2007) (and references therein). In the first model we make the simple but unrealistic assumption that the HI bias does not evolve with redshift and that it remains constant at the value measured locally by HIPASS (Barnes et al. 2001) in the concordance model, i.e., $b_{HI} = 0.68$ (Basilakos et al. 2007). More realistically, a second HI bias model considers the transformation of gas into stars and the gas consumption as a function of redshift. In this model HI galaxies are more biased at high redshift relative to the local value. Under the linear perturbation theory, Basilakos et al. (2007) derive the HI bias evolution to high redshift for a ΛCDM model, which is shown in Fig. 1 together with the constant bias model. We note that an independent measure of the bias of HI-selected galaxies as a function of redshift will be possible using redshift-space distortions in the survey.

4 STATISTICAL METHOD

4.1 Numerical implementation

We compute the relevant power spectra in Eqs. (3–5) using a modified version of the CROSS_CMBFAST[3] code. These modifications include the addition of our HI-galaxy redshift distribution (see §3) as well as the bias factor. The resulting selection function is split into different redshift bins for which the relevant power spectra are calculated.

We choose fiducial models that give an angular diameter distance to recombination fixed to the value from *WMAP* observations (Spergel et al. 2007) and let the dark energy parameters $\Omega_{\rm de}$, w_0, w_a and c_s^2 vary around the fiducial model. Unless otherwise indicated, the dark energy fiducial model is: $\Omega_{\rm de} = 0.705$, $w_0 = -0.8$, $w_a = 0$ and $c_s = 1$. In addition to the dark energy parameters, we assume a physical matter density of $\Omega_m h^2 = 0.126$, a physical baryonic density of $\Omega_b h^2 = 0.0223$, an optical depth to reionization of $\tau = 0.09$, a primordial power spectrum amplitude of $\Delta^2_{\mathcal{R}} = 2.02 \times 10^{-9}$ and a scalar spectral index of $n_s = 0.951$ (Spergel et al. 2007).

4.2 Forecasts for sound speed detection

In order to measure the significance of a detection of a sound speed model we utilise the Fisher information matrix. The Fisher matrix is defined as

$$F_{\alpha\beta} = -\left\langle \frac{\partial^2 \ln \mathcal{L}}{\partial\theta_\alpha \partial\theta_\beta} \right\rangle , \tag{12}$$

where $\mathcal{L}$, the likelihood, is the probability of observing the data set $\{x_1, x_2, ...\}$ for a given cosmological parameter set $\{\theta_1, \theta_2, ...\}$.

The Fisher matrix method allows us to forecast how well a survey will perform in constraining a set of cosmological parameters, by providing the minimum systematic uncertainty in each model parameter that is to be fit by the future survey data. Under the assumption that the individual parameter likelihoods approximate a Gaussian distribution, the information contained in the angular power spectra can be written as (Tegmark, Taylor & Heavens 1997)

$$F_{\alpha\beta} = f_{\rm sky} \sum_\ell \frac{(2\ell+1)}{2} \,{\rm Tr}[\mathbf{D}_{\ell\alpha} \tilde{\mathbf{C}}_\ell^{-1} \mathbf{D}_{\ell\beta} \tilde{\mathbf{C}}_\ell^{-1}] , \tag{13}$$

where the sum extends over multipoles ℓ, f_{sky} is the amount of sky covered by the survey, $\tilde{\mathbf{C}}_\ell$ is the data covariance matrix, and $\mathbf{D}_{\ell\alpha}$ is the matrix of derivatives of the angular power spectra

$$\mathbf{D}_{\ell\alpha} = \frac{\partial \mathbf{C}_\ell}{\partial\theta_\alpha}\Big|_{\theta_\alpha = {\rm fid}} \tag{14}$$

with respect to the parameters, θ_α, evaluated at the fiducial model. The data covariance matrix elements include the angular power spectra plus the noise terms. For the CMB, the noise contribution to the temperature measurement depends on the beam window function and the pixel noise of the experiment

$$\tilde{C}_\ell^{TT} = C_\ell^{TT} + w_T^{-1} B_\ell^{-2} , \tag{15}$$

where B_ℓ is the window function of the Gaussian beam and $w_T^{-1} = \sigma_{\rm p}^2\, \theta_{\rm beam}^2$ is the inverse noise weight with $\theta_{\rm beam}$ and $\sigma_{\rm p}$, respectively, the beamwidth and noise per pixel in a given frequency band. We consider a Planck-like CMB experiment that measures temperature anisotropies in two high frequency bands, 143 and 217 GHz. The details of these parameters for Planck can be found in e.g. Rocha et al. (2004) and are not presented here. As shown in TRC07, the contribution from the CMB spectrum to the detection significance is much less important compared to the cross-correlation and galaxy auto-correlation spectra. For the galaxy field, the source of noise comes from Poisson fluctuations in the number density

$$\tilde{C}_\ell^{gg} = C_\ell^{gg} + 1/\tilde{n}_A^z , \tag{16}$$

---

[3] `http://www.astro.columbia.edu/~pierste/ISWcode.html`

where $\tilde{n}_A^z$ is the galaxy number per steradian in the redshift bin of interest.

We construct our data covariance matrix by combining the observables as follows

$$\tilde{\mathbf{C}}_\ell \equiv \begin{pmatrix} \tilde{C}_\ell^{TT} & C_\ell^{gT,1} & C_\ell^{gT,2} & \dots & C_\ell^{gT,10} \\ C_\ell^{gT,1} & \tilde{C}_\ell^{gg,1} & 0 & 0 & 0 \\ C_\ell^{gT,2} & 0 & \tilde{C}_\ell^{gg,2} & 0 & 0 \\ \vdots & 0 & 0 & \ddots & 0 \\ C_\ell^{gT,10} & 0 & 0 & 0 & \tilde{C}_\ell^{gg,10} \end{pmatrix}, \qquad (17)$$

where the superscript number refers to the redshift bin and the zeros indicate no cross-correlation between the galaxy power spectra from different redshift bins. We have also assumed that there is no correlated noise between the galaxy and CMB power spectra.

Information about constraints on the cosmological parameters is contained in the derivatives in Eq. (13). We calculate these derivatives for each multipole by fitting a curve through the power spectra values as they vary as a function of the dark energy parameters w_0, w_a and $\Omega_{\rm de}$. We then numerically calculate the slope at the fiducial point. We require a precision that is less than one percent in order to measure the small variations in the cross-correlation and auto-correlation spectra. For this reason, we look at changes in the parameters that are large enough to allow a polynomial curve fitting.

We present the derivatives of the auto-correlation and cross-correlation power spectra with respect to the dark energy parameters in Fig. 2 and Fig. 3, respectively, for a series of redshift bins. We have multiplied the derivatives by the factor $(2\ell+1)^{1/2}$ to make the contribution of this product to the Fisher information matrix as a function of ℓ more evident. We note that the galaxy auto-correlation spectra contribute most of the signal in distinguishing sound speed models. This is due to the larger amplitude of the galaxy auto-correlation derivatives with respect to the dark energy parameters as compared to the cross-correlation derivatives. As we will see in the next section the cross-correlation spectra only add about ten percent of the discriminating signal. The cross-correlation signal originates from the large-scale ISW effect, thus the information from the cross-correlation spectrum is mainly available at low multipoles, $\ell \lesssim 20$, as can be seen in Fig. 3.

The power spectrum derivatives also provide insight into the covariance between the sound speed and other dark energy parameters. We observe in Fig. 2 that the derivative with respect to $\Omega_{\rm de}$ is two orders of magnitude larger than the derivative with respect to the sound speed. The larger amplitude and distinct shapes of the $\Omega_{\rm de}$ derivatives compared to the sound speed derivatives in different redshift bins breaks the degeneracy between $\Omega_{\rm de}$ and c_s. The amplitude of the change in the galaxy auto-correlation and cross-correlation spectra due to a varying equation of state (w_0 and w_a) is smaller than the change due to the dark energy density but still an order of magnitude larger than that caused by variations in c_s. In addition the characteristic shapes of the auto-correlation and cross-correlation derivatives with respect to w_0 and w_a in different redshift bins allow the degeneracy between w_0, w_a and c_s to be lifted.

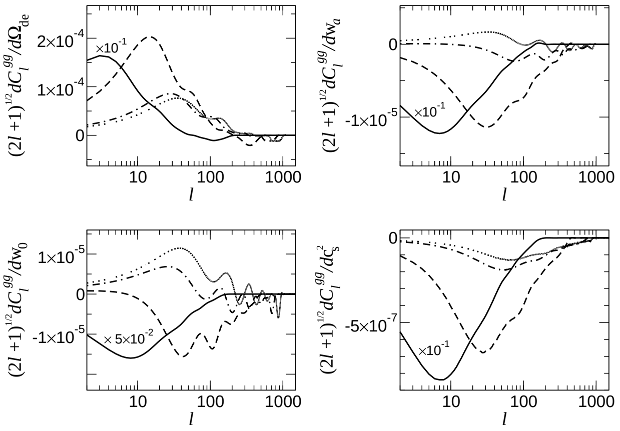

Figure 2. Derivatives of the galaxy auto-correlation power spectra with respect to the dark energy parameters $\Omega_{\rm de}$, w_a, w_0 and c_s^2 in redshift bins $0.0 < z < 0.2$ (solid), $0.4 < z < 0.6$ (dashed), $1.0 < z < 1.2$ (dot-dashed) and $1.4 < z < 1.6$ (dotted). The fiducial model used is $w_0 = -0.8$, $w_a = 0$, $\Omega_{\rm de} = 0.705$ and $c_s^2 = 1$.

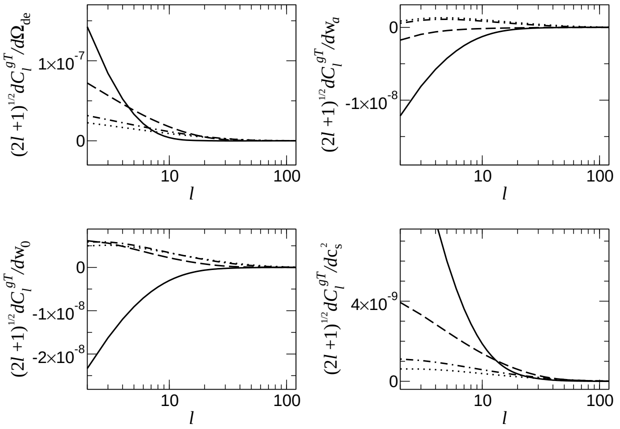

Figure 3. Derivatives of the galaxy-ISW cross-correlation power spectra with respect to the dark energy parameters $\Omega_{\rm de}$, w_a, w_0 and c_s^2 in redshift bins $0.0 < z < 0.2$ (solid), $0.4 < z < 0.6$ (dashed), $1.0 < z < 1.2$ (dot-dashed) and $1.4 < z < 1.6$ (dotted). The fiducial model is as in Fig. 2.

We extend the sum in Eq. (13) up to $\ell_{\rm max} = 1500$ to include the galaxy auto-correlation signal from the highest redshift bins, which is projected onto small angular scales.

4.3 A quantitative approach

We have seen how the use of a survey split in redshift bins helps lift the degeneracies that exist between dark energy parameters. We wish to quantify the effect on the sound speed measurement by marginalising over w_a, w_0 and $\Omega_{\rm de}$. The full Fisher matrix for this experiment includes matrix elements for all parameters

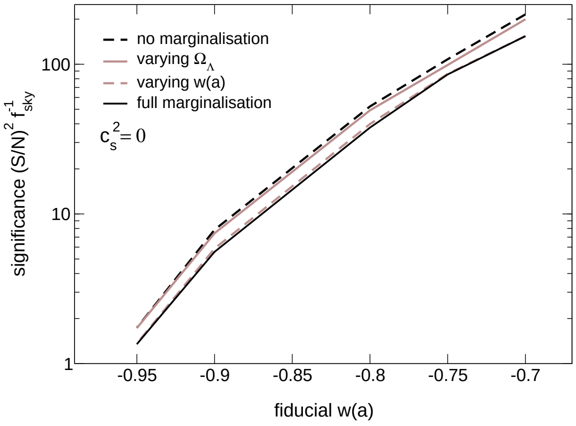

Figure 4. The significance of a detection of a $c_s^2 = 0$ dark energy model compared to a $c_s^2 = 1$ quintessence model as a function of the equation of state, $w(a)$. The S/N for a 4-hour integration per pointing is shown with all parameters fixed to fiducial values (black dashed), varying $\Omega_{\rm de}$ only (grey solid), varying $w(a)$ only (grey dashed), and full marginalisation (black solid).

$$\mathbf{F} = \begin{pmatrix} F_{cc} & \mathbf{B} \\ \mathbf{B}^T & \mathbf{A} \end{pmatrix}, \tag{18}$$

where

$$\mathbf{A} = \begin{pmatrix} F_{w_a w_a} & F_{w_a w_0} & F_{w_a \Omega_{\rm de}} \\ F_{w_a w_0} & F_{w_0 w_0} & F_{w_0 \Omega_{\rm de}} \\ F_{w_a \Omega_{\rm de}} & F_{w_0 \Omega_{\rm de}} & F_{\Omega_{\rm de}\Omega_{\rm de}} \end{pmatrix} \tag{19}$$

and

$$\mathbf{B} = \begin{pmatrix} F_{w_a c} & F_{w_0 c} & F_{\Omega_{\rm de} c} \end{pmatrix}. \tag{20}$$

We obtain the marginalised Fisher matrix by taking the inverse of $\mathbf{F}$ and extracting the sub-matrix corresponding to the parameters we want to measure. For the sound speed this is

$$(\mathbf{F}^{-1})_{11} = (F_{cc} - \mathbf{B}\mathbf{A}^{-1}\mathbf{B}^T)^{-1}, \tag{21}$$

and the marginalised Fisher matrix is the inverse of this

$$F_{\rm marg} = F_{cc} - \mathbf{B}\mathbf{A}^{-1}\mathbf{B}^T\,, \tag{22}$$

which is a scalar, since we are interested in measuring the sound speed parameter.

In order to compute the derivatives for the Fisher matrix elements involving the sound speed in Eq. (13), we note that the effect on the angular power spectra due to changes in the sound speed is only significant for order-of-magnitude variations of c_s. Following Hu & Scranton (2004), we therefore define the derivative with respect to c_s^2 in Eq. (14) as a finite difference

$$\mathbf{D}_{\ell\, c_s^2} \rightarrow \mathbf{C}_\ell(c_s^2 = 1) - \mathbf{C}_\ell(c_s^2 \neq 1)\,, \tag{23}$$

noting that, with this definition, the value of $F_{\rm marg}$ can be interpreted as the significance, $(S/N)^2$, of a detection of a sound speed model with $c_s^2 \neq 1$ relative to a quintessence model with $c_s^2 = 1$.

5 RESULTS

5.1 Signal to noise of dark energy sound speed detection

The basic detection level of a $c_s^2 = 0$ model relative to a $c_s^2 = 1$ model is shown in Fig. 4 as a function of the equation of state, w_a. It is clear that the significance of a sound speed detection is larger for models with a larger constant equation of state. This results from the fact that a component with a larger constant equation of state is more like matter, hence variations in its sound speed produce larger observable effects. For models with $w_0 \gtrsim -0.9$ the squared signal to noise exceeds 10 suggesting that these models can produce a detectable effect.

Fig. 4 also illustrates the effect of the covariance between the sound speed and other dark energy parameters. We note that the full covariance degrades the sensitivity to the sound speed but not significantly; in the absence of covariance with all other dark energy parameters the sound speed constraints improve by at most twenty percent. The lack of severe degradation in the sensitivity, that one would expect to arise from degeneracies between the dark energy parameters, is the result of information gained from measuring the auto-correlation and cross-correlation spectra in several redshift bins. We note that the sound speed covariance with the equation of state parameters, w_0 and w_a, degrades the sensitivity more than the covariance with the density $\Omega_{\rm de}$, a result that was anticipated from studying the power spectrum derivatives in the previous section.

The significance of detection of dark energy models with $c_s^2 < 1$ relative to a quintessence model with $c_s^2 = 1$ is shown in Fig. 5 for a fiducial equation of state, $w(a) = -0.8$. It is clear that the sound speed detection is most significant for dark energy models with $c_s \rightarrow 0$ as the dark energy clustering is most pronounced in these models, and becomes marginal for models with $c_s \gtrsim 0.1$. We also note that the effect of the covariance with other dark energy parameters on the sound speed measurement is most evident for models that have a high significance of sound speed detection, and hardly noticeable for models in which the sound speed is poorly measured.

We next consider the impact of the uncertainty in our HI bias model on the sound speed constraints. In Fig. 6 we compare the detection significance as a function of the sound speed for our two HI bias models. The constant bias model, which is unlikely to be realistic, predicts lower source counts at high redshift. Nevertheless this model has a sensitivity to the sound speed that is only about ten percent worse than the sensitivity of the evolving bias model. This indicates that the uncertainty in the HI bias does not change our forecasts significantly.

Finally, we have explored how the survey depth affects the significance of sound speed detection. In Fig. 6 we consider the significance of detection for a 4-hour-per-pointing survey compared to a 36-hour-per-pointing survey. We have assumed that both surveys cover the same fraction of the sky so that the 36-hour-per-pointing survey takes nine times longer to complete. The longer survey is unlikely to be practical in terms of total integration time but provides a useful guide as to how significant a much deeper survey will be for constraining the sound speed. From Fig. 6 it is clear that the deeper survey is able to discriminate more easily be-

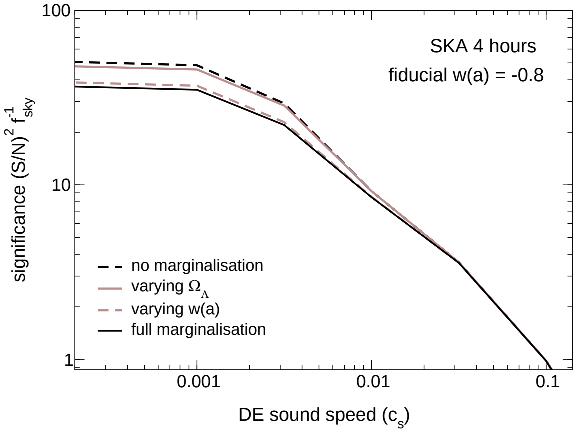

Figure 5. The significance of separation between dark energy models with $c_s^2 \neq 1$ and quintessence ($c_s^2 = 1$) for a fiducial $w = -0.8$ model of dark energy. The S/N for a 4-hour integration per pointing is shown with all parameters fixed to fiducial values (black dashed), varying $\Omega_{\rm de}$ only (grey solid), varying $w(a)$ only (grey dashed), and full marginalisation (black solid).

tween sound speed models. The signal to noise increases by a factor of two to three for low sound speed models but is approximately the same for models with $c_s \to 1$.

It is interesting to ask whether this improvement arises from the measurement of clustering at higher redshifts, $z \gtrsim 2$, or from the increased number counts at intermediate redshift. In Fig. 7 we plot the cumulative contribution of different redshift bins to the discriminating signal for a $c_s^2 = 0$ and $w = -0.8$ model. We note that for the fiducial 4-hour-per-pointing survey nearly all the signal accumulates by $z = 1.5$, and only ten percent of the signal comes from the cross-correlation spectra. For the deeper survey, approximately eighty percent of the information comes from $z \lesssim 1.5$. This suggests that the improved signal in Fig. 6 arises mostly from the increase in the number counts at intermediate redshifts (from $z = 0.5$ to $z = 1.5$), which results in a lower variance in Eq. 13, rather than the clustering signal at higher redshift.

6 CONCLUSIONS

We have studied the potential of large HI surveys to constrain constant sound speed models of dark energy. We investigated the covariance between the dark energy cosmological parameters, finding that uncertainties in the density of dark energy and in its equation of state will not dramatically degrade our ability to detect the sound speed. This arises because of the ability of these surveys to detect large numbers of HI galaxies in several redshift bins. The slight reduction in the signal to noise comes mostly from variations in the equation of state parameters.

We have also investigated the impact of using an ultra deep SKA-like HI redshift survey and assessed the effect of changing our HI bias model. We discovered that a deep survey of HI galaxies, with 36 hours of integration time per pointing improves constraints on the sound speed as compared with a smaller 4-hour-per-pointing survey due to the increased number counts at $z \lesssim 1.5$. A maximum redshift depth of $z_{\rm max} \approx 1.5$ provides most of the discriminating signal for both surveys. In addition, our results have not shown a strong dependence on the uncertainty in the HI bias model. These results could guide future planning for these types of survey experiments.

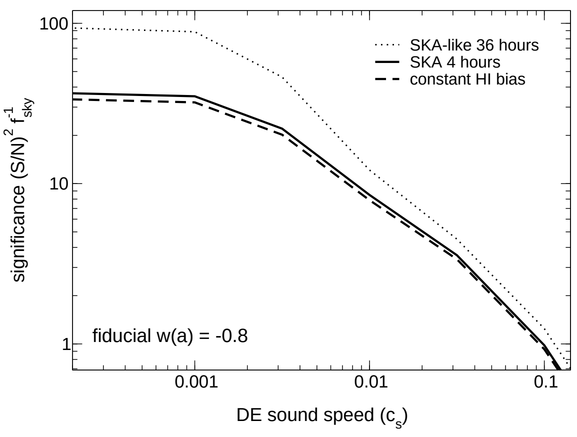

Figure 6. The significance of separation between dark energy models with $c_s^2 \neq 1$ and quintessence ($c_s^2 = 1$) for a fiducial $w = -0.8$ model of dark energy. The marginalised S/N for an SKA 4-hour-per-pointing survey (solid line) and a deeper survey of 36 hours per pointing integration time (dotted line). Both curves above are for an evolving HI bias model. The dashed line corresponds to a constant HI bias model.

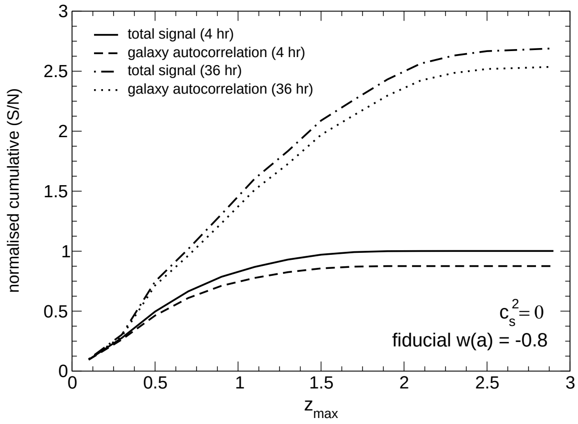

Figure 7. The cumulative significance S/N as a function of redshift contributing to the sum in Eq. (13) for a $c_s^2 = 0$ and $w = -0.8$ dark energy model. The curves are normalized to the maximum value of the total signal from the 4-hour-per-pointing survey. The dashed line represents the signal from the galaxy auto-correlation alone while the solid line represents the total signal from the auto-correlation and cross-correlation spectra. Both curves are for the 4-hour-per-pointing survey. The corresponding curves for the deeper 36-hour-per-pointing survey are shown as a dotted line (auto-correlation alone) and as a dot-dashed line (both auto- and cross-correlation).

Regarding the detection of the sound speed, we found that we can only detect models of dark energy with small values of the constant sound speed, $c_s \lesssim 0.01$. As $c_s^2 \to 0$, a model with $w = -0.9$ can be detected at the 3-σ level. For larger values of w_0 sound speeds closer to zero can be detected with greater confidence. The study of the clustering properties of dark energy through its sound speed thus promises to be an interesting approach to confront the predictions of theoretical dark energy models and uncover the nature of this mysterious component.

ACKNOWLEDGEMENTS

ATR acknowledges the SKA project office in South Africa for financial support during his PhD. KM and CC acknowledge financial support from the National Research Foundation (South Africa).

REFERENCES

Abdalla F. B., Rawlings S., 2005, MNRAS, 360, 27
Armendariz-Picon C., Mukhanov V., Steinhardt P. J., 2000, PhRvL, 85, 4438
Armendariz-Picon C., Mukhanov V., Steinhardt P. J., 2001, PhRvD, 63, 103510
Babichev E., Mukhanov V. & Vikman A, 2007, ArXiv e-prints, 708, arXiv:0708.0561
Barnes D. G. et al., 2001, MNRAS, 322, 486
Basilakos S., Plionis M., Kovač K., Voglis N., 2007, MNRAS, 378, 301
Bean R., Carroll S. & Trodden M, 2005, ArXiv Astrophysics e-prints, arXiv:astro-ph/0510059
Bean R., Doré O., 2004, PhRvD, 69, 083503
Bean R., Bernat D., Pogosian L., Silvestri A. & Trodden M., 2007, PhRvD, 75, 064020
Blake C. & Glazebrook K., 2003, ApJ, 594, 665
Bonvin C., Caprini C. & Durrer R, 2006, Physical Review Letters, 97, 081303
Bonvin C., Caprini C. & Durrer R, 2007, ArXiv e-prints, 706, arXiv:0706.1538
Caldwell R. R., Dave R. & Steinhardt P. J, 1998, Physical Review Letters, 80, 1582
Chiba T., Okabe T. & Yamaguchi M, 2000, PhRvD, 62, 023511
Chiba T, 2002, PhRvD, 66, 063514
Capozziello S., Nojiri S., Odintsov S. D., Troisi A., 2006, Phys. Lett. B639, 135
Carroll S. M, 2001, Living Reviews in Relativity, 4, 1
Carroll S. M., de Felice A., Duvvuri V., Easson D. A., Trodden M. & Turner M. S 2005, PhRvD, 71, 063513
Cooray A., 2004, MNRAS, 348, 250
Corasaniti P.-S., Giannantonio T., Melchiorri A., 2005, PhRvD, 71, 123521
Dedeo S., Caldwell R. R. & Steinhardt P. J. 2004, PhRvD, 69, 129902
Deffayet, 2001, Phys. Lett. B502, 199
Deffayet C., Dvali G. & Gabadadze G, 2002, PhRvD, 65, 044023
Dvali G., Gabadadze G. & Porrati M.,2000, Phys. Lett. B485, 208
Erickson J. K., Caldwell R. R., Steinhardt P. J., Armendariz-Picon C., Mukhanov V., 2002, PhRvL, 88, 121301
Ferreira P. G. & Joyce M, 1997, Physical Review Letters, 79, 4740
Ferreira P. G. & Joyce M. 1998, PhRvD, 58, 023503
Haiman, Z., Mohr, J. J., & Holder, G. P. 2001, ApJ, 553, 545
Hannestad S., 2005, PhRvD, 71, 103519
Hu W. & Haiman Z., 2003, PhRvD, 68, 063004
Hu W., Scranton R., 2004, PhRvD, 70, 123002
Huterer D., 2002, PhRvD, 65, 063001
Kang J. U., Vanchurin V. & Winitzki S, 2007, PhRvD, 76, 083511
Linder E. V., 2003, PhRvL, 90, 91301
Linder E. V, 2007, General Relativity and Gravitation, 181
Ma C.-P., Bertschinger E., 1995, ApJ, 455, 7
Nesseris S. & Perivolaropoulos L., 2005, PhRvD, 72, 123519
Peebles P. J. E. & Ratra B., 1988, ApJL, 325, L17
Perlmutter S. et al., 1999, ApJ, 517, 565
Péroux C., McMahon R. G., Storrie-Lombardi L. J., Irwin M. J., 2003, MNRAS, 346, 1103
Peterson J. B., Bandura K. & Pen U. L., 2006, ArXiv Astrophysics e-prints, arXiv:astro-ph/0606104
Ratra B. & Peebles P. J. E., 1988, PhRvD, 37, 3406
Riess A. G. et al., 1998, AJ, 116, 1009
Rocha G., Trotta R., Martins C. J. A. P., Melchiorri A., Avelino P. P., Bean R., Viana P. T. P., 2004, MNRAS, 352, 20
Scherrer R. J, 2004, PhRvL, 93, 011301
Scherrer R. J, 2006, PhRvD, 73, 043502
Song Y.-S. & Knox L., 2004, PhRvD, 70, 063510
Spergel D. N. et al., 2007, ApJS, 170, 377
Takada M. & Jain B., 2004, MNRAS, 348, 897
Tegmark M. et al., 2006, PhRvD, 74, 123507
Tegmark M., Taylor A. N., Heavens A. F., 1997, ApJ, 480, 22
Torres-Rodríguez A., & Cress C. M., 2007, MNRAS, 376, 1831
Weinberg S., 1989, Reviews of Modern Physics, 61, 1
Weller J., Lewis A. M., 2003, MNRAS, 346, 987
Weller J., Battye R. A. & Kneissl R., 2002, PhRvL, 88, 231301
Weller J. & Albrecht A., 2002, PhRvD, 65, 103512
Wetterich C., 1988, Nuclear Physics B, 302, 668